Production of singly charged fullerenelike fragment ions in a fast He^{2+}-C_{60} collision

Yoichi Nakai,[1] Tadashi Kambara,[1] Akio Itoh,[2] Hidetsugu Tsuchida,[3] and Yasunori Yamazaki[1]
[1]*RIKEN (The Institute of Physical and Chemical Research), Wako, Saitama 351-0198, Japan*
[2]*Quantum Science and Engineering Center, Kyoto University, Kyoto 606-8501, Japan*
[3]*Department of Physics, Nara Women's University, Nara 630-8506, Japan*
(Received 22 March 2001; published 13 September 2001)

We measured singly charged fullerenelike fragment ions by high-resolution time-of-flight (TOF) mass spectroscopy in collisions of 10 MeV He^{2+} with C_{60}. The experimental TOF spectrum was compared with Monte Carlo simulations based on the statistical C_2 emission model using two different combinations of transition states and activation energies of fullerene ions. When a very loose transition state and high activation energy of fullerene ions (9.5 eV for C_{60}^+) are used, the simulation successfully reproduces the experimental spectrum. This indicates that the dominant process of production of singly charged fullerenelike fragments is sequential C_2 emission, clearly supporting the combination of higher activation energies and a very loose bound transition state.

DOI: 10.1103/PhysRevA.64.043205 PACS number(s): 36.40.Qv, 34.50.Gb, 34.90.+q

I. INTRODUCTION

Collision-induced fragmentation and ionization of C_{60} have been intensively studied in the last ten years. In particular production processes of singly charged fullerenelike fragment ions (FLFI's) have been investigated using various techniques, such as low-energy electron impact, nanosecond-pulse laser irradiation, and low-energy collision of C_{60} ions with atoms and surfaces [1–21]. Hvelplund *et al.* proposed sequential C_2 emission as a production mechanism for FLFI's in collision of C_{60}^+ with gaseous targets [1]. Märk and co-workers showed in their electron-impact experiments that sequential C_2 emission dominates over C_4 emission for C_{56}^+ production [3,4].

In collisions of fast ions with velocities much larger than the Bohr velocity, FLFI production can be considered to proceed in the following way. First, valence electrons of C_{60} are excited by the projectile ion, and then the C_{60} ion is vibrationally excited via electron-phonon coupling. Finally, FLFI production occurs via sequential C_2 emission from the excited C_{60} ion. This situation is similar to femtosecond laser irradiation [22]. In this high-velocity region, however, few measurements of FLFI's have been performed so far [23,24], and the FLFI production mechanism is not well understood.

Below and near the Bohr velocity, a few studies of singly charged FLFI production have been performed. In these studies, sequential C_2 emission was assumed and an energy transfer to the vibrational modes of C_{60} ions was argued. Using He ions of velocities $v=0.1-1$ a.u., Schlathölter *et al.* suggested that FLFI production is induced by direct vibrational excitation [25]. On the other hand, for H^+ ions of $v=0.2-3.5$ a.u., Opitz *et al.* claimed that FLFI production is induced by vibrational excitation due to electron-phonon coupling after electronic excitation even in the low-velocity region ($v<1$ a.u.) [26]. They extracted internal-energy distributions of parent C_{60} ions from intensities of FLFI's using the simple Rice-Ramsperger-Kassel theory and the sequential C_2 emission model. Their electronic energy loss estimated by a conventional calculation agreed with the extracted internal energy of parent C_{60} ions at $v<1$ a.u.

In addition to FLFI production, investigations of the activation energy of C_2 emission for C_{60}^+ have been extensively performed experimentally and theoretically [3–8,10,11,27–29]. Experimental values before 1998 are around 5–8 eV [3–8,10,11], while quantum-chemical calculations predict higher values of about 10 eV [27–29], which seems to be more accurate as supported in recent experimental work [12,16,17]. In particular, Laskin *et al.* and Lifshitz carried out metastable-fraction measurements of FLFI's and obtained high activation energies for C_{48}^+–C_{60}^+ ions (9.5 eV for C_{60}^+) using a microcanonical dissociation model including radiative cooling of fullerene ions [16,30].

The time-of-flight (TOF) spectral profile of FLFI's has information about various physical quantities related directly to the fragmentation mechanism, such as reaction rates, activation energies, internal-energy distributions of the parent C_{60} ions, and so on. Such quantities can be studied using high-resolution TOF spectroscopy, which has, however, not been performed so far to our knowledge. We have performed such a high-resolution study of the FLFI production by 10 MeV He^{2+} ions of velocity about 10 a.u. In this paper, we present high-resolution data of the TOF spectrum measured in the mass range from C_{50}^+ to C_{58}^+. We also carried out simulations of this TOF spectrum using a sequential C_2 emission model based on the Rice-Ramsperger-Kassel-Marcus (RRKM) formalism [31]. It is shown that the present experimental result strongly supports the combination of high activation energies and a very loose transition state [16,30], indicating that the dominant process in singly charged FLFI production is sequential C_2 emission in fast-ion collisions.

II. EXPERIMENT

In Fig. 1, a schematic drawing of our experimental setup is shown. The measurements were performed with 10 MeV He^{2+} ions provided by the RIKEN Linear Accelerator (RILAC). The ion beam was well collimated to about 2×2 mm^2 upstream of a C_{60} vapor target. The C_{60} target was prepared by evaporating C_{60} powder (99.98% purity) at

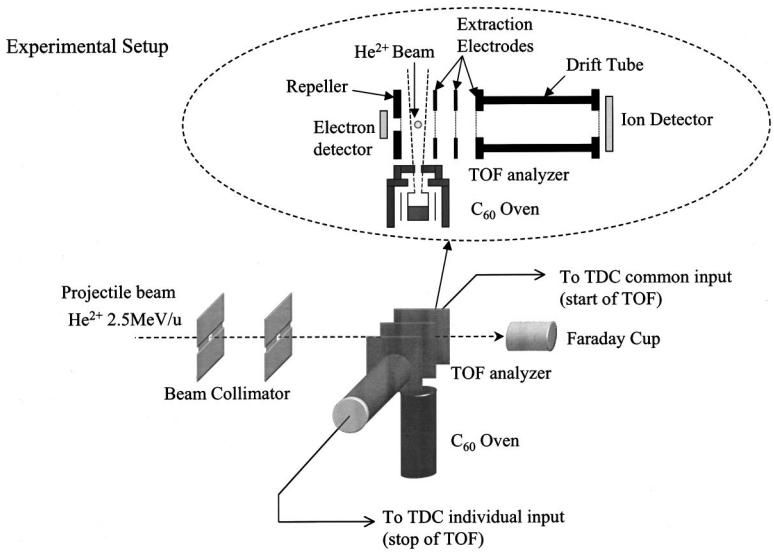

FIG. 1. A schematic drawing of our experimental setup.

500 °C in a temperature-controlled oven. The effusive C_{60} beam was introduced into the collision region through a hole (1 mm in diameter) at the top of the oven and collimated by an aperture (3 mm in diameter) located 34 mm under the He-ion beam. The incident beam and the C_{60} beam crossed each other at right angles. Residual gas pressure in the collision chamber was kept below 2×10^{-8} Torr during the experiment. The mass-to-charge ratio (m/q) of each ion produced was determined with the time-of-flight method. Electrons emitted from C_{60} were extracted from the collision region and were used as the start signal for the TOF measurement. The electron detector was a two-stage multichannel plate (MCP) with an active diameter of 14 mm. The TOF mass spectrometer was designed to fulfill the Wiley-McLaren spatial-focusing condition [32]. The bias voltages to the repeller and extractor electrodes were adjusted so as to minimize the TOF peak width of the $^{12}C_{60}{}^{+}$ ion. Extraction electric fields of 190 (2 cm) and 620 V/cm (1 cm) were used in the first and the second extraction regions of the TOF mass spectrometer, respectively. The extracted ions entered a field-free drift tube of 15 cm. After passing through the drift tube, ions were accelerated again toward a 40-mm-diam three-stage MCP with an entrance voltage of -5 kV. Each detector has an impedance-matched anode for a fast timing read out. TOF spectra were obtained using an 8-hit time-to-digital converter (TDC, LeCroy 4208). The successive signal-pulse separation of our measurement system is 20 ns due to the dead time of the discriminator.

In Fig. 2, TOF spectra of $C_{60}{}^{q+}$ $(q=1,2,3)$ are shown in order to demonstrate the TOF resolution of the present setup. Each TOF spectrum consists of several peaks corresponding to $(^{12}C_{60-n}{}^{13}C_n)^{q+}$ ions with different numbers of ^{13}C atoms. Intensity ratios among these C_{60} peaks are consistent with what are expected from the natural abundance of carbon isotopes. Each peak has a finite width, which may be attributed to fluctuation of the timing detection and thermal motion of the target C_{60}. The effect of the first is independent of m/q, and the timing detection resolution is estimated to be only 2 ns from the peak widths of $^{12}C_{60}{}^{q+}$ $(q=1,$ 2, and 3). We suppose that the m/q-dependent part arises mainly from the target thermal motion.

The detection efficiencies of $C_{60}{}^{q+}$ ions were determined from measurements of intensity variation of C_{60} ions as a function of energy impinging on the MCP front plate in the same way as in Ref. [33]. At the impinging energy of $5\times q$ keV, detection efficiencies of the ion detector were approximately 0.75, 0.95, and unity for $q=1$, 2, and 3, respectively. The efficiency for $q=1$ is much higher than the 0.4 used in [24,33], in which two-stage MCP's were used. We assumed that the detection efficiencies for $C_n{}^{q+}$ $(n=50-58)$ are the same as those for C_{60} ions with the same charge state [19].

III. TOF SPECTRUM OF SINGLY CHARGED FLFI'S

Figure 3 shows an experimental TOF spectrum in the range from $C_{50}{}^{+}$ to $C_{60}{}^{+}$. Roughly speaking, the peak intensities of $C_{60-2n}{}^{+}$ $(n=1-5)$ decrease exponentially with increasing n (see Fig. 5 below). This is consistent with other

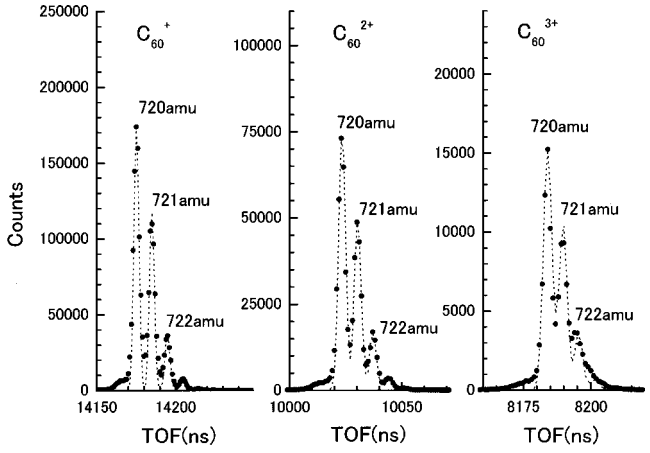

FIG. 2. TOF spectra for $C_{60}{}^{q+}$ $(q=1,2,3)$ are shown. Solid circles correspond to experimental results. Dotted lines correspond to simulation results. (See text.)

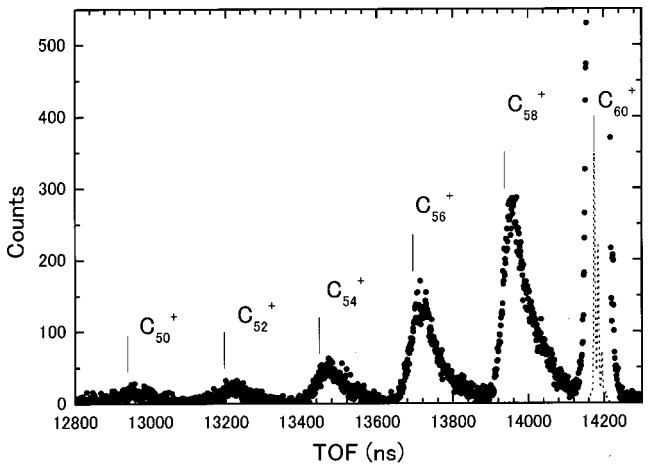

FIG. 3. Experimental TOF spectrum is shown for the TOF ranges from C_{50}^+ to C_{60}^+. The dotted line corresponds to experimental data multiplied by 0.002. Short vertical lines represent the estimated TOF peak positions of $^{12}C_{60}^+$ and $^{12}C_{60-2n}^+$ assuming that they are produced simultaneously with ionization.

studies of singly charged FLFI production [1,23–25,34]. Each peak of FLFI is more than five times wider than that of C_{60}^+ and its tail on the longer TOF side is found to curve much more gently than that on the shorter TOF side. This asymmetry becomes less prominent with lighter fragment ions. As discussed below, these wide and asymmetric peak shapes arise from the fragmentation mechanism. They arise neither from a mixture of C_{60} with a different number of ^{13}C nor from the thermal motion of the target C_{60}.

The short vertical lines in Fig. 3 represent the TOF peak positions of $^{12}C_{60-2n}^+$ fragments when they are produced promptly with zero recoil energy. It is seen that all the TOF peaks are not only tailed to but also shifted to the longer TOF side from the corresponding vertical lines. These features strongly indicate that the fragmentations take place after a C_{60} is ionized by a projectile ion.

IV. DISCUSSION

A. Monte Carlo simulation of C_2 emission

In order to analyze the experimental TOF spectrum, we assumed a sequential C_2 emission process from a parent C_{60}^+ ion and carried out Monte Carlo simulations using fragmentation rates calculated by RRKM theory. TOF spectra were simulated numerically by calculating the ion trajectories inside the TOF mass spectrometer. In this trajectory calculation, it is assumed that C_2 emission takes place sequentially with a mean lifetime corresponding to the inverse of the calculated reaction rate. The present simulations also included a recoil effect due to C_2 emission and the radiative cooling of the internal energy of ions produced. The calculation procedure is as follows.

First, as the initial condition of the trajectory calculation, we considered the thermal motion of target C_{60}, the geometric distributions of the incident-ion beam and the C_{60} molecular beam, and the m/q-independent fluctuation of the timing detection. The starting position of the trajectory and thermal velocity of target C_{60} for each trajectory were generated using random number generators. We also considered the effect due to uncertainties of the lengths of the acceleration regions and the drift tube. It was found that an uncertainty of several tens of micrometers gives rise to a TOF difference of several nanoseconds for $^{12}C_{60}^+$ (14 175 ns). In actual simulations, these lengths were adjusted appropriately within the uncertainties so as to reproduce the TOF peak position of $^{12}C_{60}^+$. The simulated TOF spectra of C_{60}^{q+} ($q=1,2,3$) are shown in Fig. 2, illustrating the validity of our assumptions for the initial conditions.

In the next step, fragmentation rate functions $k(E(C_n^+))$ of C_2 emission from C_n^+, where $E(C_n^+)$ is the internal energy of C_n^+, were calculated for parent C_{60} ions and all the fragment ions using the RRKM formalism [5–8,10,11] given by

$$k(E)=\frac{\alpha G^*(E-E_{\rm ac})}{hN(E)},$$

where α is the reaction path degeneracy, $G^*(E-E_{\rm ac})$ is the sum of state numbers of the transition state up to the energy $E-E_{\rm ac}$, $E_{\rm ac}$ is the activation energy of C_2 emission, $N(E)$ is the density of states of C_n^+ at internal energy E, and h is the Planck constant. α was chosen as $n/2$ for the C_n^+ dissociation. $G^*(E-E_{\rm ac})$ and $N(E)$ were evaluated using the Haarhoff approximation [35]. For simplicity, the average vibration frequency and the mean square of frequencies used in the Haarhoff expression for $G^*(E-E_{\rm ac})$ and $N(E)$ were taken as the same values as C_{60} for all other ions. The frequency of the active mode was fixed at 902 cm^{-1} for all the ions, obtained by multiplying by 0.88 the average vibration frequency of the Stanton and Newton calculation [36], following other calculations [5,8].

At each fragmentation step, a part of the internal energy of C_n^+ is converted to the kinetic energy of C_2 and C_{n-2}^+. The kinetic energy release (KER) $E_{\rm KER}(C_n^+)$ was assumed to follow a Maxwell distribution with a mean value of

$$\langle E_{\rm KER}(C_n^+)\rangle=\frac{E(C_n^+)-E_{\rm ac}(C_n^+)+E_z(C_n^+)}{3n-6},$$

where E_z is the zero-point vibration energy. The internal energy of C_{n-2}^+ is given by

$$E(C_{n-2}^+)=[E(C_n^+)-E_{\rm ac}(C_n^+)-E_{\rm KER}(C_n^+)]\frac{3(n-2)-6}{3n-7}.$$

As pointed out in [20,37,38], the radiative cooling of fullerenelike ions is an important competitive process in the statistical C_2 emission. Following Ref. [37], a continuous blackbody type of radiation was assumed as the radiative cooling mechanism, and the cooling rate is given by

$$\frac{dE}{dt}({\rm rad})=-A\sigma_{\rm SB}\epsilon T^4,$$

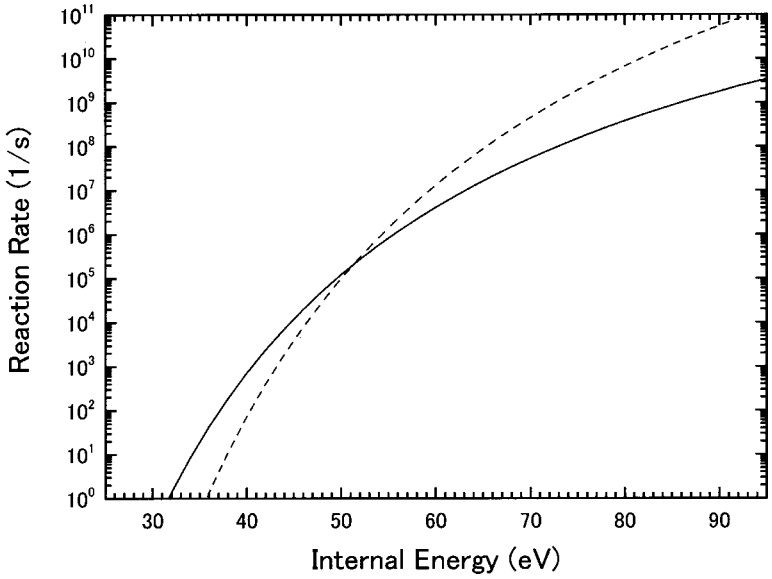

FIG. 4. Fragmentation rate functions for $C_{60}^{+} \rightarrow C_{58}^{+} + C_2$ are shown (see text). Solid line corresponds to the rate function of simulation I (the activation energy of C_{60}^{+} is 7.1 eV). Dashed line corresponds to the rate function of simulation II (the activation energy is 9.5 eV).

where A is the surface area of C_n^{+}, σ_{SB} is the Stefan-Boltzmann constant, and T is the temperature in a microcanonical ensemble of C_n^{+}. The emissivity constant $\epsilon \cong 1.4 \times 10^{-14} \times T^3$ was used, where T is measured in kelvin. The emissivity constant was estimated from the radiation intensity at 1500 K in Ref. [37]. This cooling rate is of the same order as the power loss calculated by Chupka and Klot at internal energy around 40 eV [38]. The energy loss due to radiation was subtracted from the internal energy and the dissociation rate $k(E)$ was recalculated accordingly at every time step in the trajectory calculation.

We examined two sets of activation energies E_{ac} for C_2 emission from fullerene ions. As the first set, we used an experimentally determined activation energy of 7.1 eV for C_{60}^{+} [8] and relative values with respect to 7.1 eV for other fullerene ions [14]. The simulation using this set of activation energies is referred to as simulation I.

Recently Laskin *et al.* and Lifshitz obtained high activation energies of C_2 emission from C_{48}^{+} to C_{60}^{+} (9.5 eV for C_{60}^{+}) so as to reproduce time-dependent metastable fractions and break down curves [16,30]. We used their activation energies as the second set and this simulation using the second set is referred to as simulation II. Because the transition state of C_2 emission is correlated with the activation energy, the transition state should also be reconsidered accordingly.

In Ref. [16], Laskin *et al.* reported that the transition state of C_2 emission is very loose and a corresponding Gspann parameter [39] is 33, while the Gspann parameter of about 24 is obtained for an activation energy of about 7 eV (C_{60}^{+}). Note that the Gspann parameter becomes larger with a looser transition state. Wörgötter *et al.* reported that a very loose transition state leads to high activation energies of about 9 eV for C_{60}^{+}, but they claimed that such a loose transition state is unrealistic [10]. Hansen and Campbell reported a very high Gspann parameter of 31 [20]. Matt *et al.* extracted the activation energy from their kinetic energy release measurements by assuming very high Gspann parameters of 33 and 37.6 [15,17]. Their activation energies of C_{60}^{+} and C_{58}^{+} with a very loose transition state are around 10 eV, and they are close to theoretical predictions.

In order to include a very loose transition state corresponding to high activation energies, we changed the simulation I as follows. Activation energies of C_2 emission in the reaction rate formula $k(E)$ were replaced by a second set of activation energies, but the vibration frequencies used in the Haarhoff expression of $k(E)$ were not changed. For this compensation the $k(E)$ was multiplied by 3×10^3 in order to make the calculated reaction rate of the reaction $C_{60}^{+} \rightarrow C_{58}^{+} + C_2$ close to the experimental value obtained by electron impact at an internal energy of about 50 eV [8]. If only the activation energy is changed, the calculated reaction rate becomes much smaller than the experimental one. This small reaction rate might lead to a higher internal energy for the parent C_{60}^{+} than its actual distribution. Figure 4 shows the reaction rates of C_2 emission from C_{60}^{+} for the simulations I and II.

Since our experimental result indicates that most of the fragmentations occur after C_{60} molecules have been ionized by He^{2+}-ion impact, we neglected the delayed electron emission after the sequential C_2 emission from an excited neutral parent C_{60} in our simulation. Actually, our recent TOF experiment using a chopped 10 MeV He^{2+} beam shows little component due to such delayed electron emission.

B. Comparison between simulation and experiment

In order to reduce the calculation time, we calculated trajectories only for parent C_{60}^{+} ions that have internal energies more than 35 eV because C_{60}^{+} ions with internal energy below 35 eV cannot fragment to C_{58}^{+} before entering the drift tube of our TOF analyzer. We also assumed that the functional form of the internal-energy distribution at larger than 35 eV is $f(E) = \exp(-E/E_0)$ because the internal-energy distribution of the parent C_{60}^{+} is not well known in fast-ion collisions. The adjustable parameter E_0 was determined so as to reproduce the relative yields (peak intensity ratios) from C_{50}^{+} to C_{58}^{+}. As shown in Fig. 5, we can reproduce the

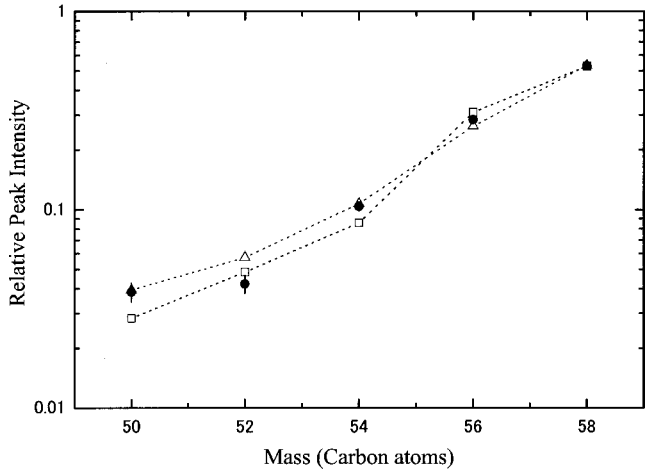

FIG. 5. Relative peak intensities from C_{50}^{+} to C_{58}^{+} are shown. Solid circles correspond to experimental results. Open squares with a dotted line correspond to the results of simulation I using the form $f(E)=\exp(-E/E_0)$ with $E_0=4.7$ eV. Open triangles with a dotted line correspond to the results of simulation II using the same form with $E_0=7.9$ eV.

relative yields fairly well using $E_0=4.7$ and 7.9 eV for the simulations I and II, respectively.

The TOF spectra of both simulations are shown in Figs. 6(a) and 6(b), respectively, where the simulated TOF spectra were normalized to the experimental one by the sum of the intensities from C_{50}^{+} to C_{58}^{+}. As shown in Fig. 6(a), simulation I does not agree with the experimental result, namely, all simulated peaks are much wider than the corresponding experimental peaks and the peak positions are shifted to the longer TOF side. In contrast to simulation I, we get fairly good agreement between the experimental TOF spectrum and simulation II. In particular, the tail at the longer TOF side and the peak position for each fragment ion are reproduced very well. However, the tail at the shorter TOF side is somewhat sharp.

As shown for C_{60}^{+} in Fig. 4, the reaction rate in simulation II decreases more rapidly with decreasing internal energy than simulation I. Also, the loss of internal energy in C_2 emission in simulation II is larger than in simulation I. Therefore, we suppose that the metastable C_2 emission with several microseconds lifetime, which makes a tail at the longer TOF side of each peak, is suppressed in simulation II and the steep peaks observed experimentally are reproduced very well.

It was also found that the simulated TOF spectrum without radiative cooling is similar to that with radiative cooling. This indicates that our TOF profile measurement is insensitive to radiative cooling compared to the metastable-fraction measurement. The reasons are that the present measurement is sensitive to the fragmentation of C_{60}^{+} with internal energy of more than about 45 eV (up to about 80 eV) and that the C_2 emission dominates over the radiative cooling in this region [16,30]. In contrast, the present measurement is sensitive to the activation energies and transition state as shown here.

We also carried out the simulation assuming another form $f(E)=E\exp(-E/E_0)$ for the internal-energy distribution of

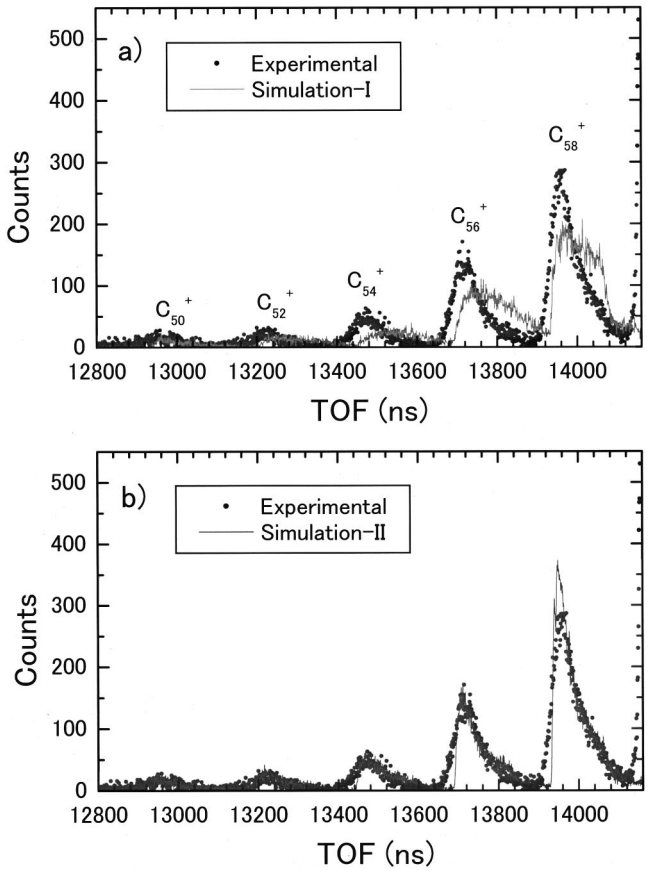

FIG. 6. Comparison of the experimental TOF spectrum with simulation results is shown. Solid circles correspond to the experimental result. Solid lines correspond to the simulation results. (a) The result of simulation I using the form $f(E)=\exp(-E/E_0)$ with $E_0=4.7$ eV for the internal energy of parent C_{60}^{+} ions before fragmentation. (b) The result of simulation II using the same form with $E_0=7.9$ eV for the internal energy of parent C_{60}^{+} ions before fragmentation.

parent C_{60}^{+} ions. In simulation I the relative yields can be reproduced well using $E_0=4.4$ eV; but the experimental TOF spectrum could not be reproduced. On the other hand, both the relative yields and the TOF spectrum can be reproduced very well using $E_0=6.9$ eV in simulation II. In the internal-energy region where the present measurement is sensitive, it was found that the internal-energy distribution in terms of this functional form is similar to that in terms of the above-mentioned exponential form for simulation II.

The present result clearly supports high activation energies and a very loose transition state. It also indicates that the dominant process of singly charged fullerenelike fragment production is the sequential C_2 emission in collisions with very fast He^{2+} ions. The peak shapes of multiply charged FLFI's are very similar to those of singly charged FLFI's. This implies a very loose transition state for the C_2 emission of multiply charged FLFI's as reported for the C_2 emission from C_{58}^{q+} $(q=1,2,3)$ by Foltin *et al.* [15].

V. SUMMARY

We applied high-resolution TOF spectroscopy to measure singly charged fullerenelike fragment ions in collisions of

C_{60} with 10 MeV He^{2+}. The time resolution of the TOF analyzer was good enough to separate the peak at 720 amu, $^{12}C_{60}{}^{+}$, from that at 721 amu, $(^{12}C_{59}{}^{13}C)^{+}$. Each peak of fullerenelike fragment ions is skewed to the longer TOF side. We simulated the TOF spectrum based on the statistical C_2 emission model using two sets of combinations of transition states and activation energies. As for the internal-energy distribution of parent $C_{60}{}^{+}$ ions, we assumed simple functional forms so as to reproduce the peak intensity ratios among fullerenelike fragment ions. When the conventional transition state and activation energies (7.1 eV for $C_{60}{}^{+}$) are used, the simulated TOF spectrum does not agree with the experimental TOF spectrum. On the other hand, when a very loose transition state and high activation energies (9.5 eV for $C_{60}{}^{+}$) [16,30] are used, the simulation successfully reproduces the experimental spectrum. Thus, the present result clearly supports high activation energies and a very loose transition state and indicates that the dominant process of production of singly charged fullerenelike fragments is the sequential C_2 emission in collisions with very fast He^{2+} ions.

ACKNOWLEDGMENT

We would like to thank the staff members of RILAC for preparing a beam for our experiment, and also for their support.

[1] P. Hvelplund, L. H. Andersen, H. K. Haugen, J. Lindhard, D. C. Lorents, R. Malhotra, and R. Ruoff, Phys. Rev. Lett. **69**, 1915 (1992).
[2] C. Lifshitz, Mass Spectrom. Rev. **12**, 261 (1993).
[3] P. Scheier, B. Dünser, R. Wörgötter, D. Müigg, S. Matt, O. Echt, M. Foltin, and T. D. Märk, Phys. Rev. Lett. **77**, 2654 (1996).
[4] M. Foltin, O. Echt, P. Scheier, B. Dünser, R. Wörgötter, D. Müigg, S. Matt, and T. D. Märk, J. Chem. Phys. **107**, 6246 (1997).
[5] R. D. Beck, J. Rockenberger, P. Weis, and M. M. Kappes, J. Chem. Phys. **104**, 3638 (1996).
[6] P. Wurz and K. R. Lykke, J. Phys. Chem. **96**, 10 129 (1992).
[7] R. K. Yoo, B. Ruscic, and J. Berkowitz, J. Chem. Phys. **96**, 911 (1992).
[8] M. Foltin, M. Lezius, P. Scheier, and T. D. Märk, J. Chem. Phys. **98**, 9624 (1993).
[9] E. Kolodney, A. Budrevich, and B. Tsipinyuk, Phys. Rev. Lett. **74**, 510 (1995).
[10] R. Wörgötter, B. Dünser, P. Scheier, T. D. Märk, M. Foltin, C. E. Klots, J. Laskin, and C. Lifshitz, J. Chem. Phys. **104**, 1225 (1996).
[11] J. Laskin and C. Lifshitz, Chem. Phys. Lett. **277**, 564 (1997).
[12] K. Hansen and O. Echt, Phys. Rev. Lett. **78**, 2337 (1997).
[13] R. Wörgötter, B. Dünser, P. Scheier, and T. D. Märk, J. Chem. Phys. **101**, 8674 (1994).
[14] P. E. Barran, S. Firth, A. J. Stace, H. W. Kroto, K. Hansen, and E. E. B. Campbell, Int. J. Mass Spectrom. Ion Processes **167/168**, 127 (1997).
[15] V. Foltin, M. Foltin, S. Matt, P. Scheier, K. Becker, H. Deutsch, and T. D. Märk, Chem. Phys. Lett. **289**, 181 (1998).
[16] J. Laskin, B. Hadas, T. D. Märk, and C. Lifshitz, Int. J. Mass. Spectrom. **177**, L9 (1998).
[17] S. Matt, O. Echt, M. Sonderegger, R. David, P. Scheier, J. Laskin, C. Lifshitz, and T. D. Märk, Chem. Phys. Lett. **303**, 379 (1999).
[18] T. Fiegele, O. Echt, F. Biasioli, C. Mair, and T. D. Märk, Chem. Phys. Lett. **316**, 387 (2000).
[19] R. Ehlich, M. Westerburg, and E. E. B. Campbell, J. Chem. Phys. **104**, 1900 (1996).
[20] K. Hansen and E. E. B. Campbell, J. Chem. Phys. **104**, 5012 (1996).
[21] R. Vandenbosch, B. P. Henry, C. Cooper, M. L. Gardel, J. F. Liang, and D. I. Will, Phys. Rev. Lett. **81**, 1821 (1998).
[22] M. Tchaplyguine, K. Hoffmann, O. Dühr, H. Hohmann, G. Korn, H. Rottke, M. Wittmann, I. V. Hertel, and E. E. B. Campbell, J. Chem. Phys. **112**, 2781 (2000).
[23] S. Cheng, H. G. Berry, R. W. Dunfort, H. Esbensen, D. S. Gemmell, E. P. Kanter, and T. LeBrun, Phys. Rev. A **54**, 3182 (1996).
[24] H. Tsuchida, A. Itoh, Y. Nakai, K. Miyabe, and N. Imanishi, J. Phys. B **31**, 5383 (1998).
[25] T. Schlathölter, O. Hadjar, R. Hoekstra, and R. Morgenstern, Phys. Rev. Lett. **82**, 73 (1999).
[26] J. Optiz, H. Lebius, S. Tomita, B. A. Huber, P. Moretto Capelle, D. Bordenave Montesquieu, A. Bordenave Montesquieu, A. Reinköster, U. Wener, H. O. Lutz, A. Niehaus, M. Benndorf, K. Haghighat, H. T. Schmidt, and H. Cederquist, Phys. Rev. A **62**, 022705 (2000).
[27] R. E. Stanton, J. Phys. Chem. **96**, 111 (1992).
[28] C. H. Xu and G. E. Scuseria, Phys. Rev. Lett. **72**, 669 (1994).
[29] A. D. Boese and G. E. Scuseria, Chem. Phys. Lett. **294**, 233 (1998).
[30] C. Lifshitz, Int. J. Mass. Spectrom. **198**, 1 (2000).
[31] For example, P. J. Robinson and K. A. Holbrook, *Unimolecular Reactions* (Wiley-Interscience, New York, 1972).
[32] W. C. Wiley and I. H. McLaren, Rev. Sci. Instrum. **26**, 1150 (1955).
[33] A. Itoh, H. Tsuchida, T. Majima, and N. Imanishi, Phys. Rev. A **59**, 4428 (1999).
[34] Y. Nakai, A. Itoh, T. Kambara, Y. Bitoh, and Y. Awaya, J. Phys. B **30**, 3049 (1997).
[35] P. C. Haarhoff, Mol. Phys. **7**, 101 (1963).
[36] R. E. Stanton and M. D. Newton, J. Phys. Chem. **92**, 2141 (1988).
[37] J. U. Andersen, C. Brink, P. Hvelplund, M. O. Larsson, B. Bech Nielsen, and H. Shen, Phys. Rev. Lett. **77**, 3991 (1996).
[38] W. A. Chupka and C. E. Klot, Int. J. Mass Spectrom. Ion Processes **167/168**, 595 (1997).
[39] C. E. Klots, Z. Phys. D: At., Mol. Clusters **20**, 105 (1991).